Challenges and Capabilities for Inspection of Cast Stainless Steel Piping

M.T. Anderson[1], S.L. Crawford[1], S.E. Cumblidge[2], A.A. Diaz[3], S.R. Doctor[4]

1) Senior Research Scientist, Pacific Northwest National Laboratory, Richland, WA (michael.anderson@pnl.gov)
2) Scientist, Pacific Northwest National Laboratory, Richland, WA
3) Staff Scientist, Pacific Northwest National Laboratory, Richland, WA
4) Laboratory Fellow, Pacific Northwest National Laboratory, Richland, WA

ABSTRACT

Studies conducted at the Pacific Northwest National Laboratory (PNNL) in Richland, Washington, have focused on developing and evaluating the reliability of nondestructive examination (NDE) approaches for inspecting coarse-grained, cast stainless steel reactor components. The objective of this work is to provide information to the United States Nuclear Regulatory Commission[1] (US NRC) on the utility, effectiveness and limitations of NDE techniques as related to the inservice inspection of primary system piping components in pressurized water reactors (PWRs). This paper describes results from recent assessments built upon early work with low frequency ultrasonic testing (UT) coupled with synthetic aperture focusing technique (SAFT) signal processing, and has subsequently evolved into an approach using low frequency phased array technology as applied from the outer diameter surface of the piping. In addition, eddy current examination as performed from the inner diameter surface of these piping welds is also reported.

Cast stainless steel (CSS) pipe specimens were examined that contain thermal and mechanical fatigue cracks located close to the weld roots and have inside/outside surface geometrical conditions that simulate several PWR primary piping weldments and configurations. In addition, segments of vintage centrifugally cast piping were also examined to understand inherent acoustic noise and scattering due to grain structures and determine consistency of UT responses from different locations. The advanced UT methods were applied from the outside surface of these specimens using automated scanning devices and water coupling. The phased array approach was implemented with a modified instrument operating at low frequencies and composite volumetric images of the samples were generated with 500 kHz, 750 kHz, and 1.0 MHz arrays. Eddy current studies were conducted on the inner diameter surface of these piping welds using a commercially available instrument and a cross point probe design operating at a frequency of 250 kHz.

Results from the laboratory studies indicate that 500 kHz phased array methods are capable of detecting flaws greater than 30% through-wall in the cast specimens. Length-sizing of flaws is possible, but no diffracted signals could be observed to support time-of-flight depth sizing. The work with eddy current examinations on the inner diameter surface indicate that, while certain cast austenitic microstructures provide excessive background noise due to permeability variations, surface-breaking flaws are quite easily detected.

INTRODUCTION

The relatively low cost and high corrosion resistance of cast stainless steel has resulted in extensive use of this material in the primary coolant piping systems of Westinghouse-designed pressurized water reactors. Alloying elements and casting processes used in the fabrication of CSS materials are responsible for its corrosion resistance and strength but also create complex and coarse-grained microstructures. This material is anisotropic and inhomogeneous. The manufacturing process can result in the formation of columnar (dendritic) grain structures often several centimeters in length, with grain growth oriented along the direction of heat dissipation, typically normal to the surface. Additionally, during the cooling and solidification process, columnar, equiaxed (randomly speckled microstructure), or a mixed structure can result, depending on chemical content, control of the cooling, and other variables in the casting process. The outer-diameter (OD) and inner-diameter (ID) surfaces of specimens used in the current study possess relatively smooth, machined conditions; this is a normal part of the fabrication method, performed to remove imperfections resulting from the casting process.

CSS piping is subjected to periodic ultrasonic testing (UT) based on requirements found in the American Society of Mechanical Engineers (ASME) Boiler and Pressure Vessel Code, Section XI, *Rules for Inservice Inspection of Nuclear Power Plant Components* [1]. For ISI to be successful, service-induced flaws must be found and repaired prior to becoming of such size that the integrity of a component is challenged. Detection of flaws is the initial priority, and for UT this is accomplished by analyzing ultrasonic echo waveforms from reflections within the volume of inspected material that could potentially be caused by service degradation. Due to the large size of the anisotropic grains, relative to the acoustic pulse

[1] This work was sponsored by the U.S. Nuclear Regulatory Commission under Contract DE-AC06-76RLO 1830; NRC JCN Y6604; Mr. Wallace Norris, NRC Project Monitor.

wavelength, the ultrasound is severely attenuated, scattered and changes in velocity are evident. Refraction and reflection of the sound beam occur at the grain boundaries, resulting in defects being incorrectly reported, specific volumes of material not being examined, or both. To reduce the impact of the microstructure on the inspection technique, the work reported here focuses on low-frequency (500 kHz to 1.0 MHz) ultrasonic energy propagation through the material as applied from the OD surface.

PNNL also evaluated the applicability and effectiveness of an inside-surface inspection technique based upon the premise that if access to the ID surface were readily available, a direct contact methodology that is sensitive to surface-breaking cracks would have an inherently higher probability of success for detection than conducting inspections from the OD. In support of this hypothesis, ID eddy current test (ET) protocols have been employed successfully in Sweden in blind test qualifications and on primary piping nozzle-to-pipe welds at the V.C. Summer Nuclear Station in the United States [2]. The objectives of the eddy current work presented are to study the use of advanced eddy current probe configurations that provide sensitivity to both axially and circumferentially oriented, near-surface flaws and to investigate the reliability and effectiveness of an inside-surface inspection technique.

To assess the affects of varied grain structures on low-frequency UT beam propagation in CSS piping and on eddy current response, vintage materials that represent those installed in the primary piping circuit at commercial operating plants were evaluated. Flaw detection and sizing were evaluated on a series of mechanical and thermal fatigue cracks in welded specimens.

EQUIPMENT

The ultrasonic phased array and eddy current systems each employed computer controlled linear X-Y scanners for data acquisition. The specific configurations for each inspection system follow.

Phased Array System

The phased array system at PNNL includes a Tomoscan III 32-channel instrument produced by ZETEC, Inc. (formerly R/D Tech, Inc.). Multiple line scans with beam direction perpendicular to the weld and scan direction parallel to the weld were acquired at varied distances from the weld centerline to create a comprehensive dataset. Delay laws were calculated to focus the sound field at approximately 60 mm (2.4 in.) into the material, and the insonification angle was swept from 30° to 60° in increments of 1° as the probe was scanned across the specimen.

Three phase array probes were used in this study, operating at 500 kHz, 750 kHz and 1 MHz. The longer the wavelength, the easier the sound can propagate through the large grains. However, the larger wavelengths have a lower resolution than shorter wavelengths. The 500 kHz-probe has a 4 x 8 matrix of piezo-composite elements and a 50% bandwidth. The higher-frequency phased arrays used include a 1.0-MHz, 2 × 11 matrix with an 88.4% bandwidth and a 750-kHz, 2 × 11 matrix with a 58.8% bandwidth. In all cases, the probes were pulsed with a square wave of approximately 500 nanoseconds duration or pulse width, which is the proper pulse width for a 1.0-MHz probe but this was the longest pulse duration allowed by the phased array system employed. This means that the full bandwidth of the 500-kHz and 750-kHz arrays could not be attained. Theoretical simulations for the 500-kHz array show a primary beam diameter of approximately 20 mm. The 750-kHz array exhibits a slightly narrower beam, with a diameter of 17 mm, and the 1.0-MHz array has a theoretical beam width of 14 mm. Lateral resolution is a function of beam width.

Eddy Current System

The eddy current examinations in this study were implemented using a ZETEC MIZ27-SI eddy current instrument and a ZETEC differential plus-point® probe (Model Z0000857-1) configured with two small coils oriented 90º to each other. As such this probe is responsive to both circumferential and axially oriented flaws. Data was acquired at test frequencies of 100, 250 and 500 kHz. The nominal operating frequency of the probe is 240 kHz thus producing the best results at 250 kHz. Only 250 kHz data is reported in this paper. This probe has a spot size of 12.5 mm and at 250 kHz produces a depth of penetration of 0.9 mm. These types of probes are generally insensitive to extraneous factors and most effective for detection of cracks and other surface material discontinuities. These operational characteristics permit the suppression of localized geometry variations (curved surfaces, corners, weld splatter) and variations in material composition (filler metals, heat-affected zone). Plus-point probes are less sensitive to permeability changes as well and can therefore be employed on both ferromagnetic and non-ferromagnetic materials.

CAST STAINLESS STEEL SPECIMENS

Vintage base metal specimens from Electric Power Research Institute (EPRI), Westinghouse, Inc., and IHI Southwest Technologies, Inc. were used to assess the affects of varied grain structure on the nondestructive evaluation. These base material specimens were without flaws. Specimens containing flaws included 15 welded piping segments on loan to PNNL

from EPRI that were fabricated to be typical of primary coolant loop components in Westinghouse-designed plants and a number of PNNL segments. These Westinghouse Owners Group (WOG) specimens contain surface-breaking thermal or mechanical fatigue cracks (TFC or MFC, respectively) on either side of the weld. The PNNL specimens, originally fabricated for an NRC-funded round robin exercise [3] and used in the Programme for the Inspection of Steel Components (PISC) [4] in the early to mid 1980s, contain surface-breaking TFCs, also on either side of the weld.

Unflawed Centrifugally Cast Stainless Steel (CCSS) Base Metal Material Description

The oldest vintage, or initial CCSS piping fabricated (from early- to mid-1960s), is thought to be similar to the IHI Southwest Technologies piping segment, which is 15.24 cm in axial extent by 127 cm in circumferential extent. The segment has an 8.4-cm wall thickness and is approximately 91 cm in outside diameter. It consists of coarse-grained, mixed, and banded microstructure. The next class, or intermediate vintage, of CCSS microstructures is represented by the piping segment on loan from Westinghouse, Inc. This segment is believed to have been fabricated in the late 1960s to mid-1970s and, although the microstructure is very challenging to examine, this intermediate segment shows consistent grain orientation and size throughout the circumference (as contrasted by the mixed structure of the oldest vintage material), which may indicate the casting process was becoming more refined. The Westinghouse segment is 25.4 cm in axial extent by 130 cm in circumferential length, with a 6.4-cm wall thickness and an approximately 71-cm outside diameter. This segment exhibits a coarse-grained, dendritic (columnar) microstructure with a banding condition evident as well. The most recently fabricated CCSS base material was loaned to PNNL by EPRI and was extracted from a cancelled nuclear power plant in Spain. The large blank spool piece has consistent fine-grained CCSS microstructure. The piece is 1.86 m in length, with a 6.35-cm wall thickness and an outside diameter of 86.4 cm. This segment has a relatively fine (for CCSS) equiaxed microstructure present over the entire circumference of the segment. This type of microstructure is believed to represent the latest class of CCSS piping installed in primary coolant systems of later vintage Westinghouse-designed plants (circa mid-1970s through mid-1980s).

Welded Flaw Specimen Description

Fifteen welded WOG piping specimens typical of several component configurations in the primary coolant loop of Westinghouse-designed plants contain surface-breaking thermal or mechanical fatigue cracks located on either side of a weld joining CSS to CSS or CSS to wrought stainless steel (WSS) materials. The CSS material was either centrifugally cast or statically cast stainless steel (SCSS). The flaws are planar cracks oriented parallel to the weld centerline, and perpendicular to and connected to the inside diameter surface. In general, the tightness and branched orientations of the thermal fatigue cracks make them more difficult to ultrasonically detect in comparison to the mechanical fatigue cracks. The piping configurations included CCSS pipe-to-SCSS elbow, SCSS elbow-to-WSS safe end, and CCSS pipe-to-SCSS pump nozzle with flaw depths between 13 and 42 percent through-wall.

The PNNL specimens consist of sections cut from butt-welded, 845 mm-OD, 60 mm-thick CCSS pipe. This pipe material was from two different heats of American Society for Testing and Materials (ASTM) A-351 Grade CF-8A, a centrifugally cast material [5]. One side of the weld contained columnar grained material and the other side equiaxed. These specimens contain welds approximately in the middle of each section and were made by welders qualified [6] to meet Section III requirements of the ASME Code. The weld crowns were ground relatively smooth and blended with the parent pipe. The ID surface contours are significantly smoother than those of the WOG specimens described earlier. The cracks in these pipe sections are thermal fatigue planar cracks, parallel to the weld centerline and perpendicular to and connected to the ID. Flaw depths were estimated based on crack growth cycles and ranged from 10 to 48 percent through-wall. Two PNNL specimens from the earlier PNNL conducted Piping Inspection Round Robin (PIRR) [3] were destructively analyzed for flaw sizing confirmation. One of the samples was 7 percent below expected crack depth while the other was 48 percent low.

Material Grain Size

Cross sections in the circumferential-radial plane of the unflawed piping segments were polished, etched, and photographed to document the grain structures in these materials. The photographs were enlarged and used to determine average grain-size measurements via the lineal intercept method. Measurements of the intercepted grains along a circumferential line were averaged to assess approximate grain size by region. The EPRI base material had a grain size range of 0.5 - 7.4 mm, the IHI Southwest material a range of 0.2 – 25.0 mm, and the Westinghouse material a range of 0.64 – 16.32 mm. The flawed specimens were examined along an axial plane with the Westinghouse flawed specimens having a range of 0.21 – 26.67 mm and the PNNL flawed specimen a range of 0.6 – 12 mm. In general, grains in the range of 12-15 mm in diameter are found for the SCSS, while 17-20 mm grains are typical for the CCSS.

PHASED ARRAY ANALYSES

A metric for establishing background noise levels due solely to the microstructure was determined by measuring the signal response from the end-of-block corner-trap geometry from the specimens. This essentially measures the response from a 100% through-wall flaw. The segment length exceeding a 6-dB threshold (i.e., corner signal present at 50% of screen height or greater) was determined as a percentage of total scan length and is shown in Figure 1 for representative specimens (note that 400 kHz conventional UT with synthetic aperture focused technique is also shown, but is not discussed in this paper). The corner response was best detected at 500 kHz, with the 1.0 MHz probe performance slightly better than the 750 kHz probe. Average detected lengths of the corner signal for the three frequencies are 84%, 52%, and 55%.

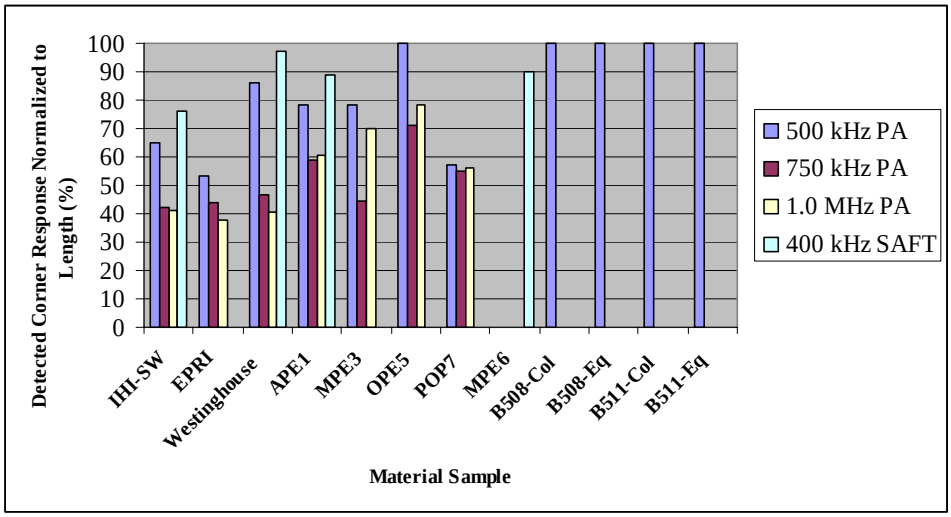

Figure 1 Detected Corner Response Values for Base Material As Determined from Inspecting the End of CCSS Specimens

The data were analyzed for flaw detection with a priori knowledge of the approximate location of each flaw relative to side of the weld and position along the weld. This study was not intended to be a blind performance demonstration but an assessment to determine the performance of low-frequency phased array technology in these coarse-grained materials. Based on analyses of data collected in this study, flaw detection is influenced by many factors including inspection frequency, side of weld inspected (i.e., near- or far-side of weld), signal-to-noise ratio, flaw area available for specular response, flaw location, flaw type, and signal discrimination in multiple images. As shown by the analysis of end-of-block corner-trap responses, acoustic scattering and beam redirection in certain microstructures may cause even the largest flaw signals to diminish over portions of their length. Therefore, large flaws thought easier to detect may be mischaracterized, and small flaws thought difficult to detect are potentially adequately imaged, depending on the microstructures present around the flaw location. Data from a detected and non-detected condition are shown in Figures 2 and 3.

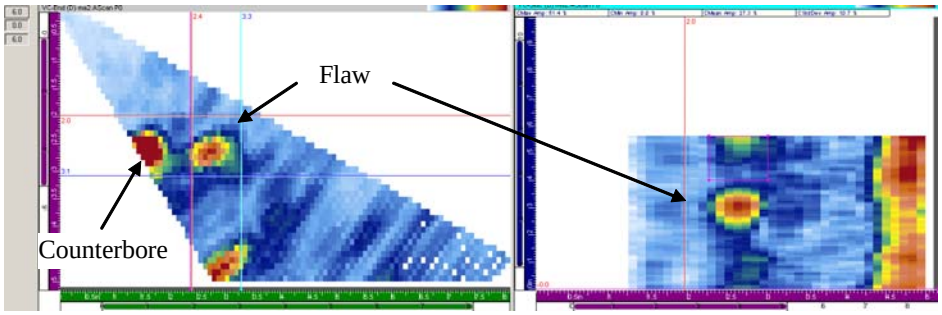

Figure 2 Mechanical Fatigue Crack in Specimen MPE-3 as Viewed From the SCSS Side at 500 kHz is Detected. Side View is on the Left and End View is on the Right.

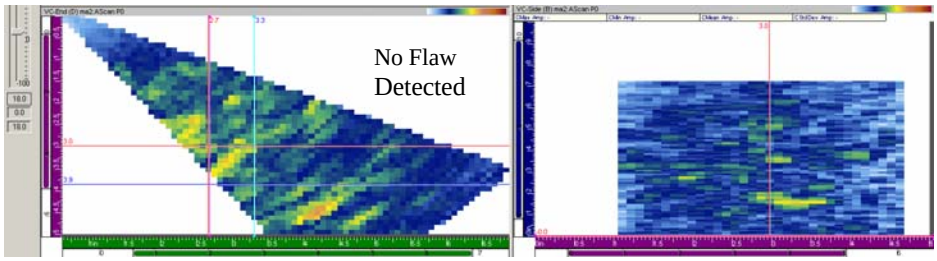

Figure 3 Mechanical Fatigue Crack in Specimen MPE-3 As Viewed from CCSS Side at 1.0 MHz is Judged To Be Not Detected. Side View is on the Left and End View is on the Right.

The summarized and tabulated results (Table 1) suggest that flaw detection is most effective when employing the 500-kHz array. Cumulative flaw detection is 71% for the given flaw types, depths, and materials. At 750 kHz, the detection rate drops to 57%, and at 1.0 MHz, the overall detection rate is 52%.

Table 1 Detection of Flaws by Type of Flaw

	Flaw Detection by Crack Type (%)		
Frequency	**Mechanical Fatigue**	**Thermal Fatigue**	**Combined**
500 kHz	93	57	71
750 kHz	64	44	57
1.0 MHz	64	33	52

Thermal fatigue cracks in these specimens are clustered in a range of approximately 20-30% through-wall in depth for WOG specimens. These thermal fatigue cracks represent the mid-range of all flaws examined and yet appear to cause the most difficulty with regard to detection. Even the smaller mechanical fatigue cracks are generally detected. Typically, cracks produced by the thermal fatigue process are tighter and more faceted than mechanical fatigue cracks, making them more difficult to detect ultrasonically, as the data in this study confirm.

Time-of-flight diffraction techniques are the only proven and acceptable methods being used in the nuclear industry for through-wall depth sizing of detected cracks. The concept is to measure the differential time for signals to be detected from the inside surface-connected portion (corner-trap response) of the flaw and the diffracted pattern produced by the flaw tip. However, throughout this study, no tip-diffracted responses from the flaws could be distinguished from baseline noise in data collected from either the CCSS or SCSS side of the welded specimens.

A length-sizing analysis was conducted with flaw length determined by the 6-dB drop and the loss of signal (LOS) techniques on the flaws. The 6-dB drop technique sets crack-length endpoints where the signal falls below a 50% level of the peak response. The loss-of-signal technique sets the endpoints where the crack signal diminishes to background noise level. The signals generally had a sharp drop-off, so the two techniques produced fairly similar results. The flaws were generally undersized which is expected from the base metal study that showed the corner signal being intermittently detected. The error calculated as the root-mean-square error (RMSE) is shown in Table 2. The 1.0-MHz transducer gives the least error. This is likely due to a smaller beam size as compared to the other two probes. Note that this error is based on detected flaws, and the 1.0-MHz transducer had the poorest detection rate. The data also show that the 500-kHz and 1.0-MHz transducers perform similarly from either the CCSS or SCSS side of the weld while the performance of the 750-kHz transducer is better from the SCSS side.

Table 2 Length Sizing of Detected WOG Flaws Using 6-dB Drop Method

	Flaw Length-Sizing Error (RMSE)		
Frequency	**CCSS**	**SCSS**	**Combined**
500 kHz	2.54 cm (1.0 in)	2.22 cm (0.87 in)	2.37 cm (0.93 in)
750 kHz	3.81 cm (1.5 in)	2.37 cm (0.93 in)	3.00 cm (1.18 in)
1.0 MHz	2.07 cm (0.81 in)	1.93 cm (0.76 in)	1.98 cm (0.78 in)

EDDY CURRENT ANALYSES

The scan area was defined as 6.35 cm on each side and parallel to the centerline of the weld and 2.54 cm from the top and bottom edges of the test specimen, to minimize the edge effects on the probe that could suppress signals from defects near the edge of the scan area. Probe sensitivity was calibrated to a 0.5-mm x 50-mm electrical discharge machining (EDM) notch, and the ET measurement system was configured to detect phase shift responses over the ranges of 65º to 105º or 245º to 285º at an operational frequency of 250 kHz using three successive sweeps and employing no amplitude threshold. Valid flaw indications resulting from planar crack-like defects had a typical phase response ranging between 65º and 105º or 245º and 285º and a length greater than 0.64 cm (0.25 in.). Indicated flaws were checked and then subsequently re-scanned to validate flaw detection

Those specimens that exhibited high noise levels in the scan area were degaussed and then re-scanned, with favorable results obtained on half of the specimens. Areas in which results were difficult to interpret were also re-scanned and categorized as hot spots. These discontinuities generally ranged between 0.64 cm and 1.0 cm in length. The general crack detection criteria employed in the analysis includes relying primarily upon the magnitude responses for detection of initial hot spots and then looking to the phase response plots for validation. The surrounding pattern of clutter and background noise must also be considered in visually discriminating between anomalous amplitude responses and those responses that are clustered and show some shape and consistent continuity. Finally, the associated length or extent is also considered, with responses less than 12.5 mm long called non-crack–like unless detected in proximity to other amplitude responses of similar intensity or where a pattern starts to develop.

Data obtained via ET techniques to characterize the ID surface of each specimen were used to plot magnitude and phase responses, generating topographical C-scan x-y representations of the data for enhanced visualization. An example of the imaged eddy current data is shown in Figure 4. In analyzing the ET data, loss of signal was used for length sizing the indications.

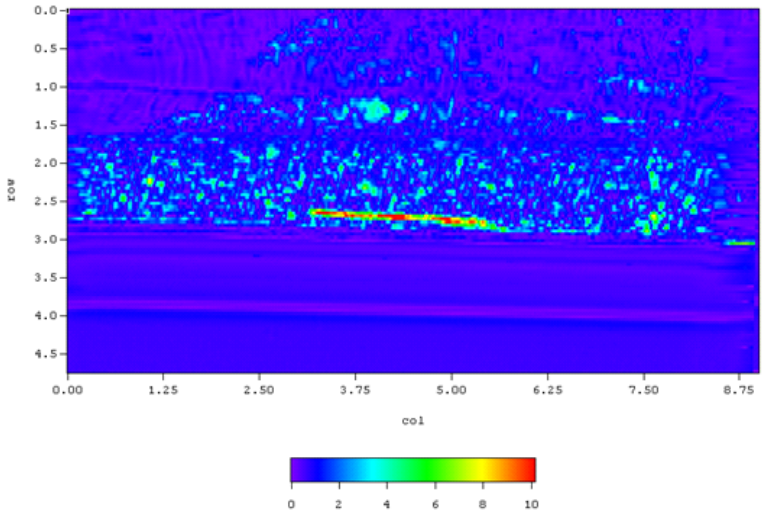

Figure 4 Degaussed Magnitude Plot of WOG Specimen INE-A-1 at 250 kHz. English units shown can be converted to metric units by multiplying by 2.54 (1 in. = 2.54 cm).

From this analysis, all 19 specimens that contained surface-breaking cracks on the inside surface were detected by the loss-of-signal methodology. With regard to length sizing, 16 of the 19 specimens containing flaws in the study were undersized, and the associated length RMSE was 7.7 mm. As the ASME Code requires the length sizing RMSE to be less than 19 mm, the ET data are well under 50% of this value. Three flaws were oversized, and the largest length difference was oversized by 3.0 mm. Noise signals having high amplitude and correct phase, and of substantial length, shape, and continuity that could be confused with crack signals, were not prevalent in the data. This study eliminated all responses less than 12.5 mm from consideration as a crack, and, as such, no false calls were reported. A review of the noise data compared to microstructural grain size and casting method (static versus centrifugal) show a direct correlation between background noise

and grain size. When comparing ET data acquired from CSS versus that from isotropic, homogeneous, fine grained material like carbon steel, a 10 to 15 dB higher level of background noise is evident in the CSS material. Slight variations in background noise were evident as a function of probe rotation relative to the orientation of the grain distribution/microstructure, but these variations were not significant.

Signal-to-noise analyses from the cracks show that mechanical fatigue cracks in the SCSS specimens exhibited signal-to-noise ratios (SNR) ranging between 8.0 dB and 11.5 dB. The ET data from thermal fatigue cracks in the SCSS specimens exhibited similar signal-to-noise ratios ranging between 10.5 dB and 11.4 dB. In contrast, for CCSS specimens, mechanical fatigue cracks in the specimens resulted in signal-to-noise ratios ranging from 14.1 dB to 16.4 dB. Also, for thermal fatigue cracks in CCSS, the ET data resulted in higher signal-to-noise ratios as well, ranging between 12.5 dB and 15.8 dB. Thus, regardless of the type of fatigue crack detected, the ET data indicate a lower overall SNR in SCSS material (by nearly a factor of 6 dB) than in CCSS material. For all CCSS specimens examined in this study (with the exception of ONP-D-2), degaussing did not improve the SNR; however, the data indicate that degaussing was generally more effective in SCSS specimens. Since the average range of grain diameters in SCSS (12 mm to 15 mm) is less than that of their CCSS counterparts (17 mm to 20 mm), with all other variables being relatively equal, this suggests that the ET SNR may be primarily driven by changes attributed to the number of grains at the surface, their orientation and the material variations in ferritic content and/or permeability, rather than sensor orientation, lift-off, geometry or crack characteristics. In the CCSS specimens studied here, the number of grain boundaries per unit area is generally less, due to their larger average grain diameter, than in SCSS, thus leading to an increase in SNR for cracks in CCSS specimens and a relative decrease in SNR for cracks in SCSS specimens.

SUMMARY AND CONCLUSIONS

The reliable volumetric examination of CSS piping in operating nuclear power plants remains a significant challenge to NDE technologies. Low-frequency UT offers the capability to penetrate relatively thick-walled sections of primary piping circuits. In this study, longitudinal waves produced by dual phased arrays operating at 500 kHz, 750 kHz, and 1.0 MHz were applied to thick-section (65–80 mm) CSS piping segments to determine whether ultrasound at these frequencies could be expected to adequately penetrate the varied microstructures and detect cracks.

It is concluded that 500-kHz large-aperture phased arrays are capable of detecting ID-connected cracking in heavy-walled CSS piping when inspected from the OD surface of the pipe. The results show that for inside surface-breaking thermal and mechanical fatigue cracks greater than approximately 30% through-wall in depth, the 500-kHz method detected 100% of the flaws, provided that access to the outside surface was sufficient for adequate transducer placement and coupling. Further, cracks smaller than 30% through-wall could also be periodically detected with the 500-kHz phased array method. No through-wall sizing of flaws was performed due to an absence of tip-diffracted responses. Length sizing is possible, although the RMSE is slightly higher than currently allowed by the ASME Code, Section XI, Appendix VIII, Supplements 2 and 3. Many industry personnel have argued that current NDE technologies are not capable of inspecting cast austenitic piping materials. This study strongly refutes that contention and provides evidence that automated low-frequency PA methods, while not fully explored, have the potential to detect and length-size cracks in CSS reactor primary coolant piping welds.

Overall, the ET methodology applied to the ID surface was very effective with regard to detection performance in that all of the cracks were detected. In summary, if the inner surface is accessible, the ET method demonstrated here is very effective for detection of surface-breaking cracks. It should be noted that this technique provided valuable detection capabilities and length sizing (within ASME Code requirements) but will not provide depth sizing information. The crack identification criteria employed in this study essentially eliminated all responses less than 12.5 mm (0.50 in.) from consideration as a crack, and as such, no false calls were reported from these data. Both magnitude and phase response information provided value in detecting cracks in these materials, while demagnetization enhanced overall SNR in approximately 42% of the specimens.

REFERENCES

1 ASME, 2004, Section XI, “Rules for Inservice Inspection of Nuclear Power Plant Components.” ASME Boiler and Pressure Vessel Code – An International Code, American Society of Mechanical Engineers, New York.

2 Rao GV, DE Seeger, Jr, C DeFlitch, JA Hoffman, RA Rees, and WR Junker, 2001, “Metallurgical Investigation of Cracking in the Reactor Vessel Alpha Loop Hot Leg Nozzle to Pipe Weld at the V. C. Summer Nuclear Generating Station,” WCAP-15616, Westinghouse Electric Company LLC, Pittsburgh, Pennsylvania.

3 Heasler PG and SR Doctor, 1996, “Piping Inspection Round Robin,” NUREG/CR-5068, PNNL-10475, U.S. Nuclear Regulatory Commission, Washington, D.C.

4 Bates DJ, SR Doctor, PG Heasler, and E Burck, 1987, “Stainless Steel Round Robin Test: Centrifugally Cast Stainless Steel Screening Phase,” NUREG/CR-4970, PNL-6266, PISC III Report No. 3. Pacific Northwest Laboratory, Richland, Washington.
5 ASTM International, 1997, “Metals Test Methods and Analytical Procedures, Volume 03.03, Nondestructive Testing.”, Section 3 in Annual Book of ASTM Standards, American Society for Testing and Materials, West Conshohocken, Pennsylvania.
6 Diaz AA, SR Doctor, BP Hildebrand, FA Simonen, GJ Schuster, ES Andersen, GP McDonald, and RD Hasse, 1998, “Evaluation of Ultrasonic Inspection Techniques for Coarse-Grained Materials”, NUREG/CR-6594, PNNL-11171, U.S. Nuclear Regulatory Commission, Washington, D.C.